ELSEVIER

Journal of Nuclear Materials 271&272 (1999) 321–325

journal of nuclear materials

Section 12.4. H, He effects and temperature transient effects

Effects of He implantation on radiation induced segregation in Cu–Au and Ni–Si alloys

A. Iwase [a,b,*], L.E. Rehn [a], P.M. Baldo [a], L. Funk [a]

[a] *Materials Science Division, Argonne National Laboratory, 9700, S. Cass Avenue, Argonne, IL 60439, USA*
[b] *Japan Atomic Energy Research Institute, Tokai-Mura, Naka-Gun, Ibaraki 319-11, Japan*

Abstract

Effects of He implantation on radiation induced segregation (RIS) in Cu–Au and Ni–Si alloys were investigated using in situ Rutherford backscattering spectrometry during simultaneous irradiation with 1.5-MeV He and low-energy (100 or 400-keV) He ions at elevated temperatures. RIS during single He ion irradiation, and the effects of pre-implantation with low-energy He ions, were also studied. RIS near the specimen surface, which was pronounced during 1.5-MeV He single-ion irradiation, was strongly reduced under low-energy He single-ion irradiation, and during simultaneous irradiation with 1.5-MeV He and low-energy He ions. A similar RIS reduction was also observed in the specimens pre-implanted with low-energy He ions. The experimental results indicate that the accumulated He atoms cause the formation of small bubbles, which provide additional recombination sites for freely migrating defects.

1. Introduction

As freely migrating defects (FMD), i.e., those vacancy and interstitial defects which escape from cascade damage and become free to migrate over distances large relative to cascade dimensions, induce microstructural changes during irradiation at elevated temperatures, it is quite important to study their behavior in order to understand the damage development in materials for fusion reactors. Recently, we have found that the cascade remnants, i.e., vacancy and/or interstitial clusters, generated by high-energy recoils act as additional recombination sites for FMD, resulting in a reduction of steady-state FMD concentrations and strong suppression of radiation induced segregation (RIS) to the specimen surface [1–3].

In first wall materials for fusion reactors, which will be exposed to 14-MeV neutrons, as well as cascade damage, helium atoms produced by (n, α)-reactions will play a critical role in microstructural changes. Much work on He effects on radiation damage has been performed, but mainly using transmission electron microscopy (TEM). With respect to the effects of He on RIS, Hidaka et al. [4] have shown from TEM observations that RIS of Cr and Ni atoms in an Fe–Cr–Ni model alloy is suppressed under simultaneous irradiation with 70-keV He and 1-MeV electrons, and Ezawa et al. have shown the effects of He on RIS in Ni–Si, Ni–Co and Ni–Cu alloys [5].

In this paper, we demonstrate through in situ Rutherford backscattering spectrometry that He atoms accumulated near the specimen surface strongly reduce the effective flux of FMD, causing suppression of RIS in Cu–Au and Ni–Si alloys.

2. Experimental procedure

Rutherford backscattering spectrometry (RBS) was used in-situ to measure RIS during single and simultaneous irradiation of Cu–1% Au and Ni–12.7% Si alloys with 1.5-MeV He and low-energy (100 or 400-keV) He. For the single-beam irradiations with low-energy He, RBS spectra were obtained with 1.5-MeV He at appropriate dose intervals. For the simultaneous

* Corresponding author. Tel.: +81-29 282 5470; fax: +81-29 282 6716; e-mail: iwase@popsvr.tokai.jaeri.go.jp

0022-3115/99/$ – see front matter
PII: S0022-3115(98)00746-6

irradiation studies, RBS spectra during 1.5-MeV He + low-energy He irradiation were obtained using backscattered 1.5-MeV He ions. The energy of the backscattered 100-keV and 400-keV He is too low to affect the RBS spectra from the 1.5-MeV He ions.

The cross section for Frenkel pair production and the accumulated He concentration per unit fluence averaged over the depth interval of 0–100 nm, where the RIS in the present experiment is always observed, are listed in Table 1 for each irradiation. Calculations were performed using TRIM-92 [6]. Other irradiation parameters, including ion beam currents, dpa (displacement per atom) rates and He accumulation rates are also shown. As can be seen from the table, the low-energy He irradiation is efficient for accumulating He atoms near the surface. On the other hand, the concentration of near-surface He from the 1.5-MeV beam is much smaller. 1.5-MeV He ions were used for generating FMD and also as a probe beam for RBS.

The effect of He pre-implantation on RIS in Cu–1%Au was also studied as follows. The specimen was pre-implanted with 100-keV or 400-keV He ions at 673 K and RBS measurements were performed subsequently during 1.5-MeV He irradiation.

The specimen temperature was kept at 673 K and 773 K, during irradiation and during RBS measurements for Cu–1%Au and Ni–12.7%Si, respectively. Experimental details on simultaneous irradiation, and in-situ RBS measurements and specimen preparation were described in a previous paper [2].

3. Experimental results

Due to the relatively weak interaction between self-interstitials and Au atoms, RIS in Cu–1%Au during ion-irradiation induces a depletion of Au near the surface [7]. The amount of Au depletion can be determined by taking the difference between the initial and subsequent RBS spectra for the near-surface region.

As the sink concentration remains negligibly small during 1.5-MeV He irradiation at elevated temperatures, the dose and dose-rate dependencies of Au depletion for 1.5-MeV He irradiation can be given by the form for the recombination dominant regime [2,7],

$$M_{\mathrm{He1.5}} = f(\Phi_{\mathrm{He1.5}})K_{0,\mathrm{He1.5}}^{-1/4} = h(\Phi_{\mathrm{He1.5}}^{\mathrm{cal}})\varepsilon_{\mathrm{He1.5}}^{-1/4}(K_{0,\mathrm{He1.5}}^{\mathrm{cal}})^{-1/4}, \quad (1)$$

where, $\varepsilon_{\mathrm{He1.5}}$ is the efficiency for producing FMD, $\Phi_{\mathrm{He1.5}}^{\mathrm{cal}}$ and $\Phi_{\mathrm{He1.5}} = \varepsilon_{\mathrm{He1.5}}\Phi_{\mathrm{He1.5}}^{\mathrm{cal}}$, are the calculated and the actual doses (dpa), respectively, and $K_{0,\mathrm{He1.5}}^{\mathrm{cal}}$ and $K_{0,\mathrm{He1.5}} = \varepsilon_{\mathrm{He1.5}}K_{0,\mathrm{He1.5}}^{\mathrm{cal}}$, are the calculated and actual dose-rates, respectively. If the assumption on sinks was also valid for the low-energy (100 and 400-MeV) He irradiations, the Au depletion in that case would be given by

$$M_{\mathrm{He100(400)}} = f(\Phi_{\mathrm{He100(400)}})K_{0,\mathrm{He100(400)}}^{-1/4} = h\left(\frac{\varepsilon_{\mathrm{He100(400)}}}{\varepsilon_{\mathrm{He1.5}}}\Phi_{\mathrm{He100(400)}}^{\mathrm{cal}}\right)\varepsilon_{\mathrm{He100(400)}}^{-1/4}(K_{0,\mathrm{He100(400)}}^{\mathrm{cal}})^{-1/4}. \quad (2)$$

Table 1
Irradiation parameters

Ion	Energy (keV)	Damage cross section [a] (cm^2)	He concentration per unit fluence (at.ppm/ion/cm^2)[a]	Beam current (nA)[b]	Dpa rate (dpa/s)	He accumulation rate (at.ppm/s)
Target Cu–1% Au						
He	1500	1.2×10^{-18}	1.1×10^{-16}	100	8.3×10^{-5}	–
He	100	1.2×10^{-17}	3.1×10^{-14}	10	1.1×10^{-5}	2.7×10^{-2}
				40	4.2×10^{-5}	1.1×10^{-1}
				160	1.7×10^{-4}	4.3×10^{-1}
He	400	2.9×10^{-18}	8.6×10^{-16}			
				10	2.5×10^{-6}	7.5×10^{-4}
				40	1.0×10^{-5}	3.0×10^{-3}
				160	4.0×10^{-5}	1.2×10^{-2}
Target Ni–12.7% Si						
He	1500	1.0×10^{-18}		100	6.4×10^{-5}	–
He	100	9.7×10^{-18}	2.9×10^{-14}	1	8.3×10^{-7}	2.5×10^{-3}
				4	3.3×10^{-6}	1.0×10^{-2}
				40	3.3×10^{-5}	1.0×10^{-1}

[a] Damage cross section and He concentration per unit fluence are the average values for the thickness of 0-100 nm.
[b] Beam current measured after He beam passed through 1 and 3 mm diameter aperture for 1.5-MeV He and low energy (100 and 400-keV) He, respectively.

Eqs. (1) and (2) indicate that the data points for low-energy He irradiation ($\Phi^{cal}_{He100(400)}M_{He100(400)}$) should fall on the same curve as those for 1.5-MeV He irradiation ($\Phi^{cal}_{He1.5}M_{He1.5}$) when they are transformed in the following fashion [2,7],

$$(\Phi^{cal}_{He100(400)}M_{He100(400)}) \rightarrow \left\{ \frac{\varepsilon_{He100(400)}}{\varepsilon_{He1.5}} \Phi^{cal}_{He100(400)}, \left(\frac{\varepsilon_{He100(400)}K^{cal}_{0,He100(400)}}{\varepsilon_{He1.5}K^{cal}_{0,He1.5}} \right)^{1/4} M_{He100(400)} \right\}. \quad (3)$$

To perform the above transformation, we need the value of the FMD efficiency ratios, $\varepsilon_{He100}/\varepsilon_{He1.5}$ and $\varepsilon_{He400}/\varepsilon_{He1.5}$. As it is well established that the FMD efficiency strongly depends on PKA (primary knock-on atom) energy spectrum [8], we calculated the fraction of defects produced by primary recoil events of energy less than T, $W(T)$, for 1.5-keV, 100-keV and 400-keV He irradiation. The results are shown in Fig. 1 which compares 800-keV Ar and Cu irradiations. The figure shows that the calculated PKA median energy $T_{1/2}$ is 0.76, 1.6 and 2.0 keV for 100-keV, 400-keV and 1.5-MeV He ion irradiations, respectively. From these values and the $T_{1/2}$ dependence of the FMD efficiency [8], the FMD efficiency ratios are estimated as $\varepsilon_{He400}/\varepsilon_{He1.5} = 1.0$ and $\varepsilon_{He100}/\varepsilon_{He1.5} = 2.0$. The other parameters in Eq. (3) can be obtained using Table 1.

Fig. 2 shows the amount of Au depletion measured for 100-keV and 400-keV He single-beam irradiations, which was transformed according to Eq. (3), and that for 1.5-MeV He irradiation, as a function of transformed dpa. The ratio of the amount of accumulated He to dpa (He/dpa ratio) in the near-surface region is

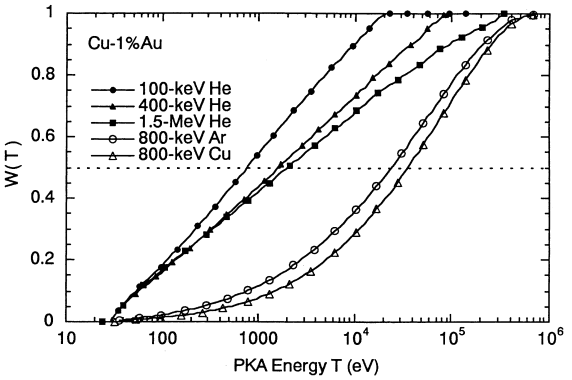

Fig. 1. Calculated fraction of defects produced by primary knock-on events of energy less than T for 1.5-keV, 100-keV and 400-keV He irradiation of Cu–1%Au. Results for 800-keV Ar and 800-keV Cu are also plotted for comparison.

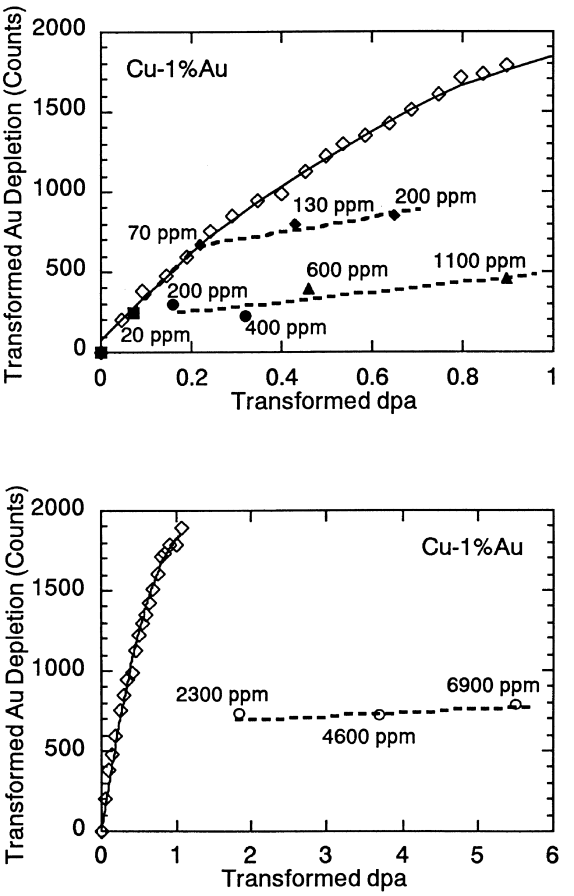

Fig. 2. Amount of near-surface Au depletion in Cu–1%Au plotted as a function of calculated dpa for 1.5-MeV He (open diamonds), 100-keV He (solid circles – 10 nA, solid triangles – 40 nA, open circles – 160 nA), and 400-keV He (solid squares – 40 nA, solid diamonds – 160 nA). Amount of Au depletion and calculated dpa were transformed using Eq. (3). Concentration of He accumulated in the near-surface region is indicated for each irradiation.

2500 at. ppm He/dpa for 100-keV He ions and 300 at. ppm He/dpa for 400-keV He ions. The concentrations of accumulated He during low-energy He irradiation are indicated in the figure. The transformed data points for low-energy He ions do not fall on the curve for 1.5-MeV He ions, but deviate toward smaller values. The deviation is quite pronounced when the He concentration becomes larger than ~100 at. ppm.

Effects of pre-implantation with low-energy He ions on the Au depletion are presented in Fig. 3. The calculated dpa and the concentration of He accumulated near the surface by pre-implantation are also shown in the figure. The data points acquired after pre-implantation do not begin at the origin, but rather at the dpa that would be required for the 1.5-MeV He irradiation to generate the same amount of Au depletion measured

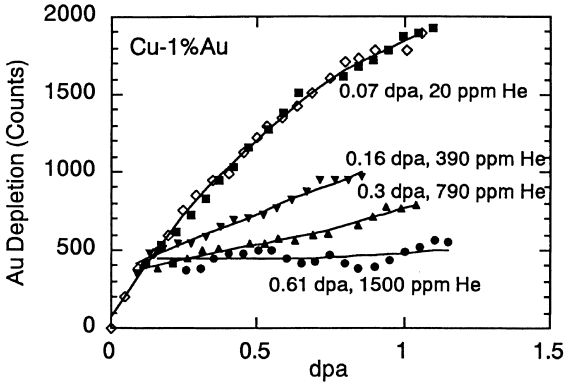

Fig. 3. Effects of pre-implantation with low-energy He on RIS in Cu–1%Au. Dpa and accumulated near-surface He following pre-implantation are indicated in the figure for each irradiation. Data points without pre-implantation are also plotted (open diamonds).

after pre-implantation. When the He concentration is small (~20 at. ppm), an effect of He on RIS cannot be observed. With increasing He concentration, the RIS suppression becomes more remarkable.

We turn next to the results for simultaneous irradiation with 1.5-MeV He and low-energy He irradiations. Fig. 4 shows the amount of near-surface Au depletion as a function of the total calculated dpa during 1.5-MeV He + 100-keV He(10 nA), and during 1.5-MeV He + 400-keV He(10 and 40 nA) simultaneous irradiations. Here the total dpa means the sum of the dpa from both beams. To compare the results for the simultaneous irradiation with that for single-beam He irradiation, all the data points for the simultaneous irradiations have been transformed in the following fashion:

$$(\Phi^{\mathrm{cal}}_{\mathrm{He100(400)+1.5He}}, M_{\mathrm{He100(400)+1.5He}}) \rightarrow \left\{ \frac{\varepsilon_{\mathrm{He100(400)+1.5He}}}{\varepsilon_{\mathrm{He1.5}}} \Phi^{\mathrm{cal}}_{\mathrm{He100(400)+1.5He}}, \left(\frac{\varepsilon_{\mathrm{He100(400)_{+1.5}He}} K^{\mathrm{cal}}_{0,\mathrm{He100(400)+1.5He}}}{\varepsilon_{\mathrm{He1.5}} K^{\mathrm{cal}}_{0,\mathrm{He1.5}}} \right)^{1/4} M_{\mathrm{He100(400)+1.5He}} \right\}, \quad (4)$$

where $\Phi^{\mathrm{cal}}_{\mathrm{He100(400)+1.5He}} = \Phi^{\mathrm{cal}}_{\mathrm{He100(400)}} + \Phi^{\mathrm{cal}}_{\mathrm{He1.5}}$, $K^{\mathrm{cal}}_{0,\mathrm{He100(400)_{+He1.5}}} = K^{\mathrm{cal}}_{0,\mathrm{He100(400)}} + K^{\mathrm{cal}}_{\mathrm{He1.5}}$, and $\varepsilon_{\mathrm{He100(400)+He1.5}} = (\varepsilon_{\mathrm{He100(400)}} K^{\mathrm{cal}}_{0,\mathrm{He100(400)}} + \varepsilon_{\mathrm{He1.5}} K^{\mathrm{cal}}_{0,\mathrm{He1.5}})/K^{\mathrm{cal}}_{0,\mathrm{He100(400)+He1.5}}$.

In the figure, the He/dpa ratio for each irradiation is shown. With increasing He/dpa ratio, the RIS suppression becomes stronger. Even when the total near-surface He concentration does not exceed ~30 at. ppm, RIS is strongly suppressed.

In the case of higher He/dpa ratios, the RIS suppression is more pronounced. Fig. 5 shows the Au depletion measured during 1.5-MeV He + 100-keV He(40 nA) and 1.5-MeV He + 100-keV He(160 nA) simultaneous irradiations as a function of dpa only by the 100-keV He ions (not the total dpa!). The He/dpa ratio is 880 ppm He/dpa and 1700 ppm He/dpa, respectively. The rate of Au depletion per dpa by 100-keV He for simultaneous irradiation is the same as that for the 100-keV He single-beam irradiation. This result implies that the RIS from the 1.5-MeV He ions is completely suppressed by simultaneous 100-keV He irradiation, i.e., only the RIS due to the 100-keV He ion beam is observed.

Simultaneous irradiations with 1.5-MeV and 100-keV He were performed also on Ni–12.7%Si, where the

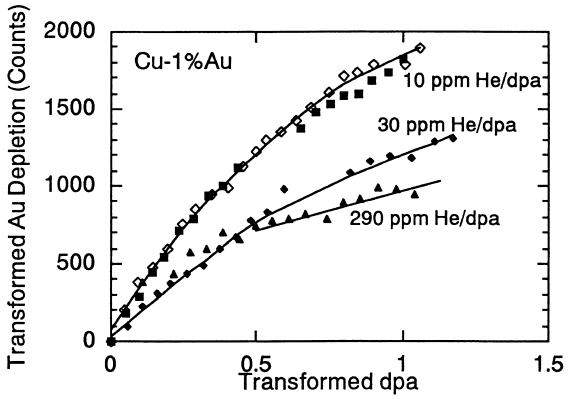

Fig. 4. Amount of near-surface Au depletion in Cu–1%Au plotted as a function of calculated dpa for 1.5-MeV He irradiation (open diamonds), simultaneous irradiation with 1.5-MeV and 100-keV He (solid triangles – 10 nA), and simultaneous irradiation with 1.5 -MeV He and 400-keV He (solid diamonds – 40 nA, solid squares – 10 nA). Dpa and amount of Au depletion for simultaneous irradiation are transformed using Eq. (4).

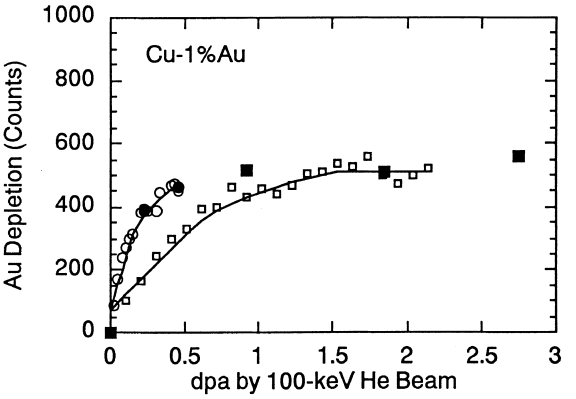

Fig. 5. Amount of near-surface Au depletion in Cu–1%Au plotted as a function of dpa calculated for only the 100-keV He beam, for simultaneous irradiation with 1.5-MeV He and 100-keV He (open circles – 40 nA, open squares – 160 nA). Results for 100-keV He single-beam irradiation (solid circles – 40 nA, solid squares – 160 nA) are also shown.

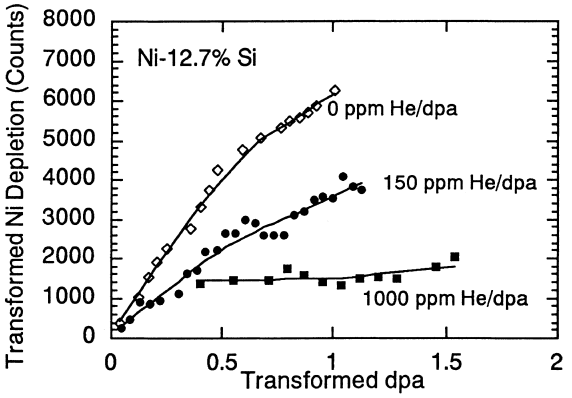

Fig. 6. Amount of near-surface Ni depletion in Ni–12.7%Si plotted as a function of calculated dpa for 1.5-MeV He irradiation (open diamonds) and simultaneous irradiation with 1.5-MeV and 100-keV He (solid circles – 4 nA, solid squares – 40 nA). Amount of Ni depletion and dpa are transformed using Eq. (4).

RIS appeared as an enrichment of Si atoms, and relative depletion of Ni, near the surface [9]. As can be seen in Fig. 6, the RIS suppression during the simultaneous 1.5 and 100-keV He irradiations occurs in the same manner as for the Cu–1% Au alloy.

4. Discussion

As shown in Section 3, RIS in Cu–1%Au and Ni–12.7%Si is strongly suppressed by low-energy (100 or 400-keV) He irradiation. The RIS is driven by the existence of a persistent flux of FMD to the surface. Therefore, the present result means that the low-energy He irradiation decreases the FMD flux to the surface. A similar RIS reduction has been observed in these alloys irradiated simultaneously with 1.5-MeV He and heavy-ions, or pre-irradiated with heavy-ions [1–3]. We have explained this RIS suppression as due to cascade remnants, i.e., interstitial and/or vacancy clusters, serving as additional recombination sites for FMD. In the case of low-energy He irradiation, however, the fraction of cascade remnants is much smaller than for heavy-ion irradiation, because the PKA energy spectrum is much softer as shown in Fig. 1. On the other hand, low-energy He irradiation is quite efficient at accumulating He atoms near the specimen surface. With increasing concentration of accumulated He, the RIS suppression becomes more pronounced. Therefore, we can conclude that the He atoms themselves, and not the cascade remnants, cause the RIS suppression observed in Cu–Au and Ni–Si alloys irradiated with low-energy He.

Small bubbles are generated at high densities in Cu, Ni and their alloys irradiated with He ions up to 100–200 ppm at elevated temperatures [10,11]. The present result suggests that the He bubbles act as additional recombination sites for FMD [4], resulting in the decrease of FMD flux to the surface.

Despite a large difference in defect properties, and in the kinetics of RIS, between the two alloys, the effects of He on RIS in Ni–12.7%Si are remarkably similar to those in Cu–1%Au. This similarity implies that the role of He bubbles as recombination sites for FMD is a general phenomenon through which RIS suppression can occur.

5. Summary

We have observed a strong suppression of RIS in Cu–1%Au and Ni–12.7%Si alloys during irradiation with low-energy (100 or 400-keV) He single-beam irradiation, during simultaneous irradiation with 1.5-MeV He and low-energy He, and following pre-implantation with low-energy He ions. This RIS suppression is attributed to the small He bubbles produced during low energy He irradiation, which provide additional recombination sites for FMD, and thereby reduce the flux of FMD to the surface.

Acknowledgements

The authors are grateful to B. Kestel for the expert assistance with specimen preparation. This work was supported by the US Department of Energy, BES-Materials Science under Contract No. W-31-109-ENG-38.

References

[1] A. Iwase, L.E. Rehn, P.M. Baldo, L. Funk, Appl. Phys. Lett. 67 (1995) 229.
[2] A. Iwase, L.E. Rehn, P.M. Baldo, L. Funk, J. Nucl. Mater. 238 (1996) 224.
[3] A. Iwase, L.E. Rehn, P.M. Baldo, L. Funk, J. Nucl. Mater. 244 (1997) 147.
[4] Y. Hidaka, S. Ohnuki, H. Takahashi, S. Watanabe, J. Nucl. Mater. 212–215 (1994) 330.
[5] T. Ezawa, E. Wakai, T. Tanabe, R. Oshima, J. Nucl. Mater. 191–194 (1992) 1346.
[6] J.P. Biersack, L.G. Haggmark, Nucl. Instrum. Meth. 174 (1980) 257.
[7] T. Hashimoto, L.E. Rehn, P.R. Okamoto, Phys. Rev. B 38 (1988) 12868.
[8] L.E. Rehn, H. Wiedersich, Mater. Sci. Forum 97–99 (1992) 43.
[9] L.E. Rehn, P.R. Okamoto, R.S. Averback, Phys. Rev. B 30 (1984) 3073.
[10] S.J. Zinkle, R.A. Dodd, G.L. Kulcinski, K. Farrell, J. Nucl. Mater. 117 (1983) 213.
[11] V. Zell, H. Schroeder, H. Trinkaus, J. Nucl. Mater. 212–215 (1994) 358.